Redox Behavior of the Black Roussinate $[Fe_4S_3(NO)_7]^-$ Monoanion. Synthesis and Spectroscopic Characterization of the $[Fe_4S_3(NO)_7]^{n-}$ (n = 2, 3) Anions and Crystal Structures of the Mono- and Dianions in Their $[NEt_4]^+$ Salts

Sabatino D'Addario,[†] Francesco Demartin,[‡] Loris Grossi,[§] Maria Carmela Iapalucci,[†] Franco Laschi,[∥] Giuliano Longoni,*[,†] and Piero Zanello[∥]

Dipartimento di Chimica Fisica ed Inorganica, viale Risorgimento 4, 40136 Bologna, Italy, Istituto di Chimica Strutturistica Inorganica and Centro del CNR, via Venezian 21, 20133 Milano, Italy, Dipartimento di Chimica Organica, viale Risorgimento 4, 40136 Bologna, Italy, and Dipartimento di Chimica, Pian dei Mantellini 44, 53100 Siena, Italy

Received July 20, 1992

A reinvestigation of the redox behavior of $[Fe_4S_3(NO)_7]^-$ by electrochemical techniques shows the existence of a four-step electron-transfer sequence, in which the overall charge changes from -1 to -4; the reactions are electrochemically reversible, and the electrogenerated $[Fe_4S_3(NO)_7]^{n-}$ (n = 2, 3) species appear to be stable. The redox potentials (V vs SCE) in acetonitrile solution are as follows: $E_{-1/-2}$ = -0.68, $E_{-2/-3}$ = -1.26, $E_{-3/-4}$ = -1.75. Similar results have also been obtained in dichloromethane and tetrahydrofuran solutions. The $[Fe_4S_3(NO)_7]^{2-}$ species has been chemically generated by reduction of the parent monoanion with sodium naphthalenide in tetrahydrofuran, isolated in a crystalline state as the $[NEt_4]^+$ salt, and spectroscopically characterized in several solvents; the corresponding $[Fe_4S_3(NO)_7]^{3-}$ species has been obtained by reduction of the latter in hexamethylphosphortriamide with sodium and has only been spectroscopically investigated "in situ". The even-electron $[Fe_4S_3(NO)_7]^{3-}$ is EPR silent, whereas the odd-electron $[Fe_4S_3(NO)_7]^{2-}$ exhibits an EPR spectrum which suggests the presence in solution of a mixture of two paramagnetic species. Their relative abundance is mainly a function of the solvent, counterion, temperature, and time. The first species shows a signal at g = 2.020 consisting of three equally intense lines due to the coupling of the unpaired electron with a unique ^{14}N nucleus ($a(^{14}N)$ = 5.0 G). The second displays an EPR signal consisting of a 1:2:3:2:1 quintet at g = 2.026, due to the coupling with two equivalent ^{14}N nuclei ($a(^{14}N)$ = 2.7 G). EHMO calculations performed on $[Fe_4S_3(NO)_7]^-$ with an idealized C_{3v} symmetry indicate that the LUMO is doubly degenerate; these two molecular orbitals are antibonding with respect to the Fe-Fe, Fe-S, and Fe-NO interactions and receive contribution mainly from the four iron atoms and either one or the remaining two axial nitrosyl groups, respectively. Single occupation of this energy level should result into loss of degeneracy by distortion of the metal framework from C_{3v} to C_s idealized symmetry along E vibrational modes; depending on the deformation, a triplet or a quintet is to be expected in the EPR signal because of coupling of the unpaired electron with either one or two equivalent nitrogen atoms. An X-ray determination of the structure of $[Fe_4S_3(NO)_7]^{2-}$ as the $[NEt_4]^+$ salt has been achieved. (Crystal data: a = 10.248(3), b = 17.814(8), c = 18.475(4) Å; β = 103.33(3)°; space group $P2_1/c$; R = 0.045.) Comparison of its structural parameters with those of $[Fe_4S_3(NO)_7]^-$ as the $[AsPh_4]^+$ salt failed to confirm unambiguously the presence of the above distortions, probably because of the influence of packing effects. Experimental confirmation of the expected distortions has only been obtained following an X-ray redetermination of the structure of the $[Fe_4S_3(NO)_7]^-$ monoanion as its $[NEt_4]^+$ salt. (Crystal data: a = 9.161(4), b = 10.254(2), c = 13.480(4) Å; α = 97.71(2), β = 109.86(3), γ = 94.82(2)°; space group $P\bar{1}$; R = 0.018.)

Introduction

Metal-sulfur clusters generally exhibit high propensity toward multiple redox changes.[1,2] This is observed in the iron-sulfur-nitrosyl clusters[3] $Fe_4(\mu_3\text{-}S)_4(NO)_4$,[4] $Fe_4(\mu_3\text{-}S)_2(\mu_3\text{-}NCMe_3)_2(NO)_4$,[5] and $[Fe_4(\mu_3\text{-}S)_3(NO)_7]^-$,[6] which encompass the $[Fe_4(\mu_3\text{-}S)_4(NO)_4]^{0/-/2-}$, $[Fe_4(\mu_3\text{-}S)_2(\mu_3\text{-}NCMe_3)_2(NO)_4]^{0/-/2-/3-/4-}$, and $[Fe_4(\mu_3\text{-}S)_3(NO)_7]^{-/2-/3-/4-}$ redox series, respectively. Crystallographic studies on $[Fe_4(\mu_3\text{-}S)_4(NO)_4]^{n-}$ and $[Fe_4(\mu_3\text{-}S)_2(\mu_3\text{-}NCMe_3)_2(NO)_4]^{n-}$ allowed the structures of the relevant redox couples (n = 0, 1)[4,7] to be elucidated, whereas for $[Fe_4S_3(NO)_7]^{n-}$ only the structure of the monoanion has been reported.[8,9] Moreover, no EPR spectral data of the above $[Fe_4S_3(NO)_7]^{n-}$ (n = 2, 4) odd-electron species have been reported.

It was, therefore, of interest to investigate in more detail this series of compounds and also to ascertain the eventual occurrence of diradical clusters, of which very few examples are known, e.g. $Co_{3-x}M_x(\eta^5\text{-}C_5H_5)_2(\mu_3\text{-}CO)_2$ (M = Rh, Ir; x = 0-3).[10-12] Moreover, since the nitrosyl groups are suggested to be effective "electron sink" through a linear-NO^+ → bent-NO^- conversion,[13,14]

[†] Dipartimento di Chimica Fisica ed Inorganica.
[‡] Istituto di Chimica Strutturistica Inorganica and Centro del CNR.
[§] Dipartimento di Chimica Organica.
[∥] Dipartimento di Chimica.

(1) Zanello, P. *Coord. Chem. Rev.* **1988**, *83*, 199.
(2) Zanello, P. *Coord. Chem. Rev.* **1988**, *87*, 1.
(3) Butler, A. R.; Glidewell, C.; Li, M. H. *Adv. Inorg. Chem.* **1988**, *32*, 336.
(4) Chu, C. T. W.; Lo, F. Y. K.; Dahl, L. F. *J. Am. Chem. Soc.* **1982**, *104*, 3409.
(5) Gall, R. S.; Chu, C. T. W.; Dahl, L. F. *J. Am. Chem. Soc.* **1974**, *96*, 4019.
(6) Crayston, J. A.; Glidewell, C.; Lambert, R. J. *Polyhedron* **1990**, *9*, 1741.
(7) Chu, C. T. W.; Gall, R. S.; Dahl, L. F. *J. Am. Chem. Soc.* **1982**, *104*, 737.
(8) Johansson, G.; Lipscomb, W. N. *Acta Crystallogr.* **1958**, *11*, 594.
(9) Chu, C. T. W.; Dahl, L. F. *Inorg. Chem.* **1977**, *12*, 3245.
(10) Olson, W. L.; Stacy, A. M.; Dahl, L. F. *J. Am. Chem. Soc.* **1986**, *108*, 7646.
(11) Bray, A. C.; Green, M.; Hankey, D. R.; Howard, J. A. K.; Johnson, O.; Stone, F. G. A. *J. Organomet. Chem.* **1985**, *281*, C12.
(12) Hermann, W. A.; Barnes, C. E.; Zahn, T.; Ziegler, M. L. *Organometallics* **1985**, *4*, 172.
(13) Connelly, N. G. *Inorg. Chim. Acta Rev.* **1972**, 47.
(14) Richter-Addo, G. B.; Legzdins, P. *Chem. Rev.* **1988**, *88*, 991.

0020-1669/93/1332-1153$04.00/0

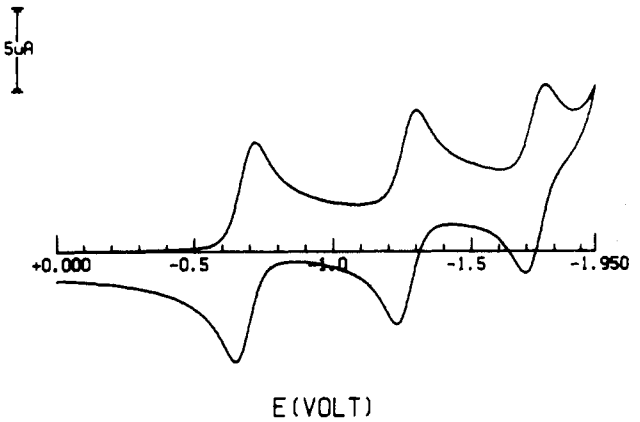

Figure 1. Cyclic voltammogranm recorded at the platinum electrode on an acetonitrile solution containing $[NEt_4][Fe_4S_3(NO)_7]$ (1.2×10^{-3} M) and NEt_4ClO_4 (0.2 M). The scan rate is 0.2 V·s^{-1}.

induced by addition of electrons,[15,16] it was of interest to ascertain experimentally to which extent the π-antibonding NO orbitals could compete with Fe–Fe antibonding orbitals as an electron sink.

We report here the results of both a chemical and electrochemical reinvestigation of the redox behavior of the black Roussinate $[Fe_4(\mu_3\text{-}S)_3(NO)_7]^-$ monoanion, the spectroscopic characterization of the $[Fe_4(\mu_3\text{-}S)_3(NO)_7]^{-/2-/3-}$ series of compounds, and a comparative structural characterization of the redox couple $[Fe_4(\mu_3\text{-}S)_3(NO)_7]^{-/2-}$, in their tetraethylammonium salts.

Results and Discussion

1. Electrochemical Behavior of $[Fe_4(\mu_3\text{-}S)_3(NO)_7]^-$. The redox fingerprint of the black Roussinate $[Fe_4(\mu_3\text{-}S)_3(NO)_7]^-$ monoanion[17-19] in acetonitrile solution is shown in Figure 1. In agreement with the previously reported brief investigations performed in dichloromethane[20] and tetrahydrofuran[6] solutions, the compound exhibits three distinct reduction processes. Controlled-potential coulometric tests performed in correspondence of the first cathodic process ($E_w = -0.85$ V) indicate that it involves the consumption of one electron per molecule. During the electrolysis no appreciable change in color of the starting red-brown solution occurs. Cyclic voltammetric tests after exhaustive electrolysis show the full chemical reversibility of the $[Fe_4(\mu_3\text{-}S)_3(NO)_7]^{-/2-}$ redox change. The same results hold as far as the second cathodic step is concerned. With respect to the color of the mono- and dianions, the solution of the electrogenerated $[Fe_4S_3(NO)_7]^{3-}$ trianion lost the red component and darkened. No attempt to electrogenerate the $[Fe_4S_3(NO)_7]^{4-}$ tetraanion has been performed because of the presence of the solvent discharge.

Analysis[21] of the cyclic voltammetric responses relevant to the first reduction process with scan rate varying from 0.02 to 10.24 V·s^{-1} showed the following: (i) The anodic-to-cathodic peak-current ratio, i_{pa}/i_{pc}, is constantly equal to 1. (ii) The current function $i_{pc} \cdot v^{-1/2}$ (v = scan rate in V·s^{-1}) remains constant. (iii) The peak-to-peak separation, ΔEp, progressively increases from 66 to 154 mV. In spite of the theoretical expectation that an electrochemically reversible one-electron transfer should display a ΔEp value of 59 mV constant with scan rate, the presence of uncompensated solution resistances could be responsible for the actual departure, which is significant only at high scan rate. This should indicate, as it will be shown later on, that no gross structural change accompanies the reduction of $[Fe_4(\mu_3\text{-}S)_3(NO)_7]^-$ to $[Fe_4(\mu_3\text{-}S)_3(NO)_7]^{2-}$. By considering that in the same scan rate range the peak-to-peak separation of the second chemically reversible cathodic step increases from 70 to 146 mV, one could foresee that also the $[Fe_4S_3(NO)_7]^{3-}$ trianion substantially maintains the geometry of the starting monoanion.

Table I. Formal Electrode Potentials (in V, vs SCE) and Peak-to-Peak Separation (in mV, at 0.2 V·s^{-1}) for the Three Successive One-Electron Additions to $[Fe_4(\mu_3\text{-}S)_3(NO)_7]^-$ in Different Nonaqueous Solutions

	−/2−		2−/3−		3−/4−		
solution	$E^{\circ\prime}$	ΔEp	$E^{\circ\prime}$	ΔEp	$E^{\circ\prime}$	ΔEp	ref
MeCN[a]	−0.68	70	−1.26	72	−1.75	78	this work
CH_2Cl_2[b]	−0.79	72	−1.33	72	−1.9	*c*	this work
	−0.89						20
THF[b]	−0.77	130	−1.35	123	−1.81	143	this work
	−0.77[d]		−1.37[d]		−1.87[d]		6

[a] $[NEt_4][ClO_4]$ (0.2 M) as supporting electrolyte. [b] $[NBu_4][ClO_4]$ (0.2 M) as supporting electrolyte. [c] Evaluation of ΔE_p was hampered by the closeness of the solvent discharge. [d] Potential values arbitrarily referenced to SCE.

The redox potentials of the consecutive redox changes $[Fe_4S_3(NO)_7]^{-/2-/3-/4-}$ are summarized in Table I and compared with the results of previous studies carried out in different solvents.[9,20] The relatively large peak-to-peak separation found in the highly resistive tetrahydrofuran has to be attributed to uncompensated solution resistances, rather than to structural variations of the depolarizer; indeed, the observed ΔEp is comparable with that found for the one-electron oxidation of ferrocene (see Experimental Section), which is known to undergo minimal structural reorganizations.

2. Isolation and Chemical Characterization of the $[Fe_4S_3(NO)_7]^{n-}$ (n = 1–3) Anions. The observation that exhaustive macroelectrolysis experiments on the $[Fe_4S_3(NO)_7]^{n-}$ (n = 1–3) redox family does not indicate any trace of decomposition led to an investigation of the related chemical reduction of $[Fe_4(\mu_3\text{-}S)_3(NO)_7]^-$ with the aim to spectroscopically and structurally characterize both the $[Fe_4S_3(NO)_7]^{2-}$ and $[Fe_4S_3(NO)_7]^{3-}$ anions.

The chemical reduction of $[Fe_4(\mu_3\text{-}S)_3(NO)_7]^-$, in its alkali,[18] ammonium,[19] or tetrasubstituted ammonium salt, has been performed with similar results both in THF and hexamethylphosphortriamide (HMPTA) by using as reducing agents stoichiometric amounts of sodium naphthalenide and sodium metal solutions, respectively. In both cases the addition of 1–1.2 equiv of sodium causes a shift of ca. 60 cm^{-1} to lower wavenumbers of the nitrosyl infrared absorptions and the progressive growth of EPR signals at g = 2.024 in THF and g = 2.026 in HMPTA, owing to progressive formation of the $[Fe_4(\mu_3\text{-}S)_3(NO)_7]^{2-}$ paramagnetic dianion (see later). On further addition of ca. 1 equiv of sodium both these solutions become EPR silent and, concomitantly, the infrared nitrosyl absorptions shift ca. 70 cm^{-1} to lower wavenumbers due to formation of the corresponding $[Fe_4S_3(NO)_7]^{3-}$ trianion. The $[Fe_4S_3(NO)_7]^{3-}$ trianion is quantitatively oxidized prior to $[Fe_4(\mu_3\text{-}S)_3(NO)_7]^{2-}$ and then to $[Fe_4(\mu_3\text{-}S)_3(NO)_7]^-$ by addition of stoichiometric amounts of several oxidizing agents such as iodine, $[Fe(\eta^5\text{-}C_5H_5)_2]Br$, and atmospheric oxygen. Combined IR, EPR, and proton NMR monitoring does not indicate formation of any species other than the above. Interestingly the $[Fe_4(\mu_3\text{-}S)_3(NO)_7]^{2-}$ paramagnetic dianion is readily regenerated from the diamagnetic $[Fe_4S_3(NO)_7]^{3-}$ trianion also by addition of wet solvents to the corresponding solutions of the later. In this reaction, EPR monitoring shows the progressive growth of the typical signal of the $[Fe_4(\mu_3\text{-}S)_3(NO)_7]^{2-}$ dianion. However, a minor signal due

(15) Lionel, T.; Morton, J. R.; Preston, K. F. *J. Phys. Chem.* **1982**, *86*, 367.
(16) Geiger, W. E.; Rieger, P. H.; Tulyathan, B.; Rausch, M. D. *J. Am. Chem. Soc.* **1984**, *106*, 7000.
(17) Roussin, M. L. *Ann. Chim. Phys.* **1858**, *52*, 285.
(18) Pavel, O. *Chem. Ber.* **1882**, *15*, 2600.
(19) Brauer, G. *Handbook of Preparative Inorganic Chemistry*, 2nd ed.; Academic Press: New York, 1965; p 1764.
(20) Wharton, E. J.; McCleverty, J. A. *Inorg. Nucl. Chem. Lett.* **1970**, *6*, 549.
(21) Brown, E. R.; Sandifer, J. R. In *Physical Methods of Chemistry Electrochemical Methods*; Rossiter, B. W., Hamilton, J. F., Eds.; J. Wiley: New York; Vol. 2, Chapter 4.

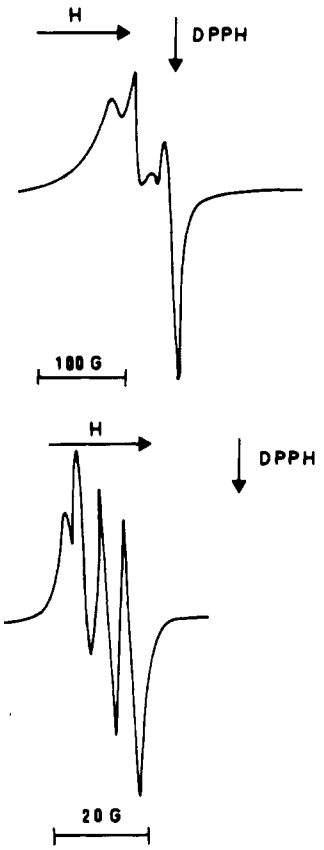

Figure 2. X-band EPR spectrum of the $[Fe_4S_3(NO)_7]^{2-}$ dianion, electrogenerated in acetonitrile solution, recorded at (a, top) 110 K and (b, bottom) room temperature.

to a yet unknown species is often also present; this essentially consists of a 1:1:1 triplet (g = 2.005; $a(^{14}N)$ = 1.6 G), each line of which shows an unresolved hyperfine structure.

In contrast, related attempts to chemically and spectroscopically investigate the $[Fe_4S_3(NO)_7]^{4-}$ species provided results of low reproducibility.

The sensitivity to humidity of $[Fe_4S_3(NO)_7]^{3-}$ and, to a lesser extent, of $[Fe_4(\mu_3\text{-}S)_3(NO)_7]^{2-}$ hampered their isolation in a solid crystalline state. Thus, the attempted metathesis of their alkali and ammonium salts with tetrasubstituted ammonium or phosphonium halides in methanol mainly gives rise to precipitation of the corresponding salts of the $[Fe_4(\mu_3\text{-}S)_3(NO)_7]^-$ monoanion, probably as a consequence of hydrolysis reactions of the polyanions and evolution of hydrogen. The above difficulty has partially been solved by using preformed tetrasubstituted ammonium salts of $[Fe_4(\mu_3\text{-}S)_3(NO)_7]^-$. For instance, treatment of $[NEt_4][Fe_4(\mu_3\text{-}S)_3(NO)_7]$ in THF solution with slightly more than 1 equiv of sodium naphthalenide in THF results into the direct separation of a microcrystalline precipitate of the sparingly soluble $[NEt_4]_2[Fe_4(\mu_3\text{-}S)_3(NO)_7]$ in ca. 40–50% yields, whereas the remaining part of the $[Fe_4(\mu_3\text{-}S)_3(NO)_7]^{2-}$ dianion stays in solution as the alkali salt. The precipitate has been crystallized by dissolution in anhydrous acetonitrile and precipitation by slow diffusion of diisopropyl ether.

Related attempts to isolate the corresponding $[Fe_4S_3(NO)_7]^{3-}$ salts by treatment of the above suspension with one further equivalent of sodium naphthalenide provided a crude product consisting mainly of salts of the trianion; unfortunately, all the attempts to grow crystals suitable for X-ray studies out of the above crude precipitate have so far been unsuccessful.

3. Spectroscopic Characterization of $[Fe_4(\mu_3\text{-}S)_3(NO)_7]^{2-}$ and $[Fe_4S_3(NO)_7]^{3-}$. The $[Fe_4(\mu_3\text{-}S)_3(NO)_7]^{2-}$ dianion in acetonitrile solution shows infrared nitrosyl absorptions at 1748 (w), 1689 (s), and 1660 (ms, sh) cm^{-1}, which can be compared with the corresponding absorptions of the parent $[Fe_4(\mu_3\text{-}S)_3(NO)_7]^-$ monoanion, which occur at 1795 (w), 1743 (s), and 1708 (w) cm^{-1}. The $[Fe_4S_3(NO)_7]^{3-}$ trianion shows infrared nitrosyl absorptions at 1696 (w), 1679 (w), 1608 (s), and 1598 (s, sh) cm^{-1}.

The EPR spectrum of a polycrystalline sample of $[NEt_4]_2[Fe_4(\mu_3\text{-}S)_3(NO)_7]$ shows an unresolved broad signal. On the contrary, the solution EPR spectrum of the paramagnetic $[Fe_4(\mu_3\text{-}S)_3(NO)_7]^{2-}$ dianion shows well-defined spectral behavior and has been investigated in several solvents (THF, acetone, acetonitrile, HMPTA) on samples generated both by electrochemical or chemical reduction of the parent monoanion, as well as on a crystalline sample of $[NEt_4]_2[Fe_4(\mu_3\text{-}S)_3(NO)_7]$ dissolved in the above solvents. We believe that the EPR spectral behavior of its solutions are at variance with the preparation procedure as a result of solvent and counterion effects.

The frozen-solution X-band EPR spectrum of the $[Fe_4(\mu_3\text{-}S)_3(NO)_7]^{2-}$ dianion electrogenerated at 253 K in acetonitrile solution is shown in Figure 2a. The spectral analysis allows one to identify two well-separated groups of EPR signals, with line shapes characteristic of different "one-electron" systems, hereafter indicated as A and B. Taking into account a $S = {}^1/_2$ spin Hamiltonian for each absorption pattern, the corresponding X-band EPR parameters can be suitably calculated as

$$g_{A\parallel} = 2.047 \pm 0.005$$

$$g_{A\perp} = 2.005 \pm 0.005$$

$$\langle g\rangle_{A(calc)} = {}^1/_3(g_\parallel + 2g_\perp) = 2.019 \pm 0.005$$

$$g_{B\parallel} = 2.014 \pm 0.005$$

$$g_{B\perp} = 2.030 \pm 0.005$$

$$\langle g\rangle_{B(calc)} = 2.025 \pm 0.005$$

The actual anisotropic spectral parameters are consistent with the presence of two species having one unpaired electron.[22] Even if at T = 110 K the overall ΔH appears to be significantly narrow for the A and B paramagnetic systems, the lack of superhyperfine splitting in glassy solution, as proved by the second derivative spectrum, can be explained with the assumption that the actual overall $\Delta H_{tot} > a(\parallel, \perp)$ of both the A and B systems. In the frozen solution the A/B molar ratio is of the order of 5:1.

Upon an increase of the temperature, at the glassy–liquid phase transition (T = 250 K) the anisotropic features drop out and a sharp and narrow 1:1:1 triplet shows up, characterized by the following parameters:

$$\langle g\rangle(250\ K) = 2.020 \pm 0.002$$

$$\langle a\rangle_t(250\ K) = 5.0 \pm 0.5\ G$$

These features are attributable to species A; furthermore the 1:1:1 intensity ratio is indicative of the superhyperfine coupling of the unpaired spin electron with a unique nitrogen atom ($I(^{14}N)$ = 1). At room temperature the overall line shape slightly broadens, this effect being particularly evident on the low-field absorptions, while the corresponding $\langle g\rangle$ and $\langle a\rangle$ parameters remain unaltered. The relevant spectrum is shown in Figure 2b. The line shape analysis indicate the presence of a minor signal partially overlapped to the low-field absorption of the triplet and centered at $\langle g\rangle(300\ K) = 2.026 \pm 0.002$, with $\Delta H(300\ K) = 2.0 \pm 0.5$ G. The g value of this signal matches that of species B;

(22) Butler, A. R.; Glidewell, C.; Hyde, A. R.; Walton, J. C. *Polyhedron* **1985**, *4*, 737 and references therein.

however its poor intensity does not allow an unambiguous attribution (see later).

Somewhat different X-band EPR features have been found in THF solution, particularly in the temperature range of the fluid solution ($T \geq 165$ K), on samples electrogenerated at 253 K in THF solution. The liquid-nitrogen overall line shape is quite similar to that found in acetonitrile solution, even if the spectral resolution of the two A and B patterns is less pronounced. In addition, there is significant evidence for a poorly resolved structure in the parallel region of the A spectrum. The corresponding A and B parameters at 110 K are

$$g_{A\parallel} = 2.049 \pm 0.002$$

$$g_{A\perp} = 2.004 \pm 0.002$$

$$\langle g \rangle_{A(calc)} = 2.019 \pm 0.002$$

$$a_{A\parallel} = 7.0 \pm 0.5 \text{ G}$$

$$a_{A\perp} = (3\langle a \rangle - a_{\parallel})/2 = 2 \pm 0.5 \text{ G}$$

$$g_{B\parallel} = 2.017 \pm 0.002$$

$$g_{B\perp} = 2.033 \pm 0.002$$

$$\langle g \rangle_{B(calc)} = 2.028 \pm 0.002$$

At the glassy–liquid transition phase, a single and unresolved absorption line is present, centered at $\langle g \rangle$(165 K) = 2.019 ± 0.005 and with ΔH(165 K) = 25.0 ± 0.5 G; at temperatures higher than 240 K the signal resolves in a complex line shape, the structure of which is noticeably temperature dependent. The spectra of $[Fe_4(\mu_3\text{-}S)_3(NO)_7]^{2-}$ at T = 275 K and 310 K, respectively, are shown in Figure 3. The spectrum at T = 275 K displays an isotropic line shape resolved into two distinct sets of multiplets; the more intense signal is a 1:1:1 triplet centered at $\langle g \rangle_t$(275 K) = 2.021 ± 0.002 ($\langle a \rangle_t$(275 K) = 4.8 ± 0.5 G), which partially overlaps to a less intense 1:2:3:2:1 quintet, centered at $\langle g \rangle_q$(275 K) = 2.026 ± 0.002 ($\langle a \rangle_q$(275 K) = 2.7 ± 0.5 G). The isotropic parameters allow the triplet structure to be attributed to species A and the quintuplet to species B, respectively. It seems evident that the quintet arises from the interaction of the unpaired electron with two equivalent nitrosyl ligands. The A:B molar ratio of 2:1 indicates that a significant increase of species B takes place with temperature. This effect is even more evident at T = 310 K, where the quintet becomes the predominant signal; at this temperature the A:B molar ratio after equilibration is of the order of 1:8.

The chemical generation of the $[Fe_4(\mu_3\text{-}S)_3(NO)_7]^{2-}$ dianion at room temperature in EPR-silent THF or HMPTA solution by reduction of the parent monoanion, respectively, with sodium naphthalenide or a sodium solution in HMPTA, gives rise to the progressive growth in the EPR of the five lines signal (g = 2.024, a = 2.7 G in THF; g = 2.026, a = 2.6 G in HMPTA) due to species B (Figure 4). The three-line signal due to A is often undetected and becomes progressively noticeable only with time to reach up to ca. 10% relative concentration. Evaporation of THF and monitoring by EPR of the residue dissolved in acetonitrile or acetone initially shows a variable mixture of A and B. On standing the relative intensity of the signals changes with time and after 24–48 h either A or B prevails, apparently as a function of the concentration of the Na^+ counterion (B being favored by the highest Na^+ concentrations). In both circumstances the final EPR signal was found substantially unaltered after standing for two additional days. Significantly, concomitant IR monitoring does not indicate any noticeable change in the nitrosyl pattern during the above transformations. The time

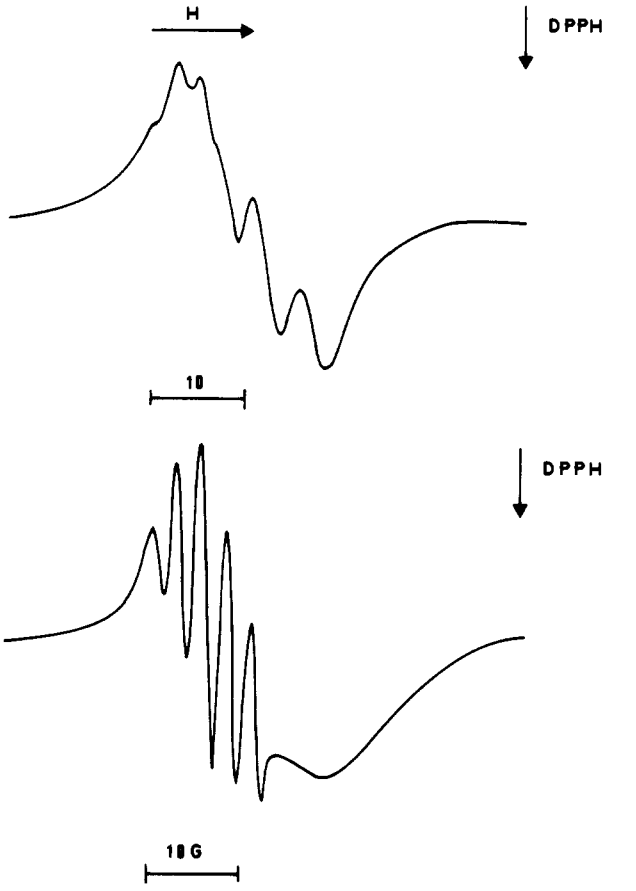

Figure 3. X-band EPR spectrum (a (top) T = 275 K; b (bottom) T = 310 K) of the $[Fe_4S_3(NO)_7]^{2-}$ dianion electrogenerated in THF solution.

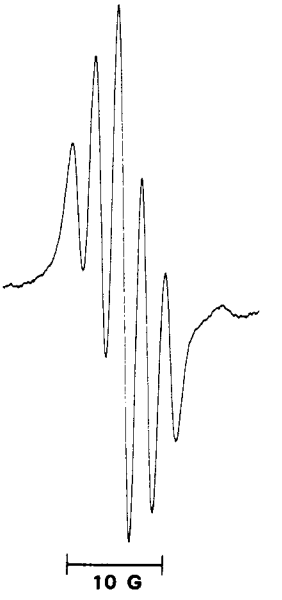

Figure 4. X-band EPR spectrum at room temperature of the $[Fe_4S_3(NO)_7]^{2-}$ dianion generated in THF solution by chemical reduction of the parent monoanion with sodium naphthalenide.

dependence of the EPR spectrum in acetonitrile solution at high concentration of Na^+ is illustrated in Figure 5.

Crystalline samples of $[NEt_4]_2[Fe_4(\mu_3\text{-}S)_3(NO)_7]$ upon dissolution in acetonitrile, acetone, and HMPTA show substantially comparable EPR features and essentially show the 1:1:1 three-line signal typical of A. Unfortunately the low solubility and/or stability of $[NEt_4]_2[Fe_4(\mu_3\text{-}S)_3(NO)_7]$ in other miscellaneous solvents has hampered a more extended investigation of the solvent effect; correspondingly, a direct investigation of the solid sample was of little use due to the lack of superhyperfine splitting.

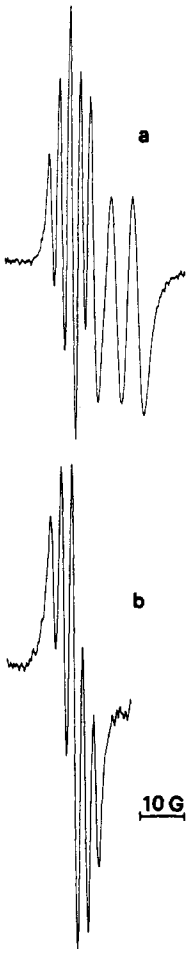

Figure 5. Time dependence of the EPR spectra of $[Fe_4S_3(NO)_7]^{2-}$ chemically generated in THF by reduction with sodium (a, after evaporation of THF and dissolution in acetonitrile; b, after 48 h).

In principle several contrasting interpretations of the above spectral behavior may appear likely: indeed the EPR patterns of A and B are not unambiguously distinctive of a $[Fe_4(\mu_3\text{-}S)_3(NO)_7]^{2-}$ paramagnetic species and could be respectively displayed by monomeric iron mono- and dinitrosyl species,[3] arising for instance from fragmentation of $[Fe_4(\mu_3\text{-}S)_3(NO)_7]^{2-}$ in the miscellaneous solvents. In keeping with this interpretation it has been reported that the parent $[Fe_4(\mu_3\text{-}S)_3(NO)_7]^-$ diamagnetic monoanion upon dissolution in dimethylformamide displays an EPR signal indicative of the presence of several paramagnetic species probably consisting of iron nitrosyl solvato complexes.[22] However, attribution of both, or even a single one of the above signals, to fragmentation products seems rather unprobable in the present case owing to the following experimental observations: (a) The EPR parameters of species A and B are very little affected by the miscellaneous solvents (in contrast, different iron–nitrosyl solvato complexes display different g values and often show further splitting due to the presence of nitrogen and/or β or γ hydrogen atoms in the donor solvent).[22] (b) The IR nitrosyl pattern is essentially invariant during the above transformations. (c) Cyclovoltammetric responses performed during exhaustive $-1/-3$ redox cyclings does not show any noticeable trace of decomposition. (d) Salts of the $[Fe_4(\mu_3\text{-}S)_3(NO)_7]^{2-}$ dianion have been isolated in a solid crystalline state from the above solutions. Therefore, it seems more likely to be able to conclude that species A and B are two isomeric forms of $[Fe_4(\mu_3\text{-}S)_3(NO)_7]^{2-}$, differently stabilized by the particular ensemble of solvent and cation, rather than two different paramagnetic compounds, one (or both) arising from fragmentation of the former. Besides, the above unexpectedly simple EPR patterns are also in keeping with the presence of an intact $[Fe_4(\mu_3\text{-}S)_3(NO)_7]^{2-}$ architecture in solution, as suggested by EHMO calculations (see later).

Table II. Fractional Atomic Coordinates of Non-Hydrogen Atoms (Esd's in Parentheses) for $[NEt_4][Fe_4S_3(NO)_7]$

atom	x	y	z
Fe(1)	0.02359(3)	0.08764(3)	0.30007(2)
Fe(2)	−0.21090(3)	−0.00858(3)	0.11259(2)
Fe(3)	0.14509(3)	0.20742(3)	0.17298(2)
Fe(4)	−0.13034(3)	0.30100(3)	0.29376(2)
S(1)	0.04823(6)	−0.00764(5)	0.15064(4)
S(2)	−0.22951(6)	0.08529(5)	0.26810(4)
S(3)	0.12938(6)	0.29801(5)	0.33121(4)
O(1)	0.1542(2)	−0.0486(2)	0.4712(1)
O(21)	−0.3462(3)	−0.2770(2)	0.0542(2)
O(22)	−0.3565(2)	0.1153(2)	−0.0624(1)
O(31)	0.4582(2)	0.2294(2)	0.1837(2)
O(32)	−0.0016(3)	0.3353(2)	0.0009(1)
O(41)	−0.2032(2)	0.4450(2)	0.4588(1)
O(42)	−0.2723(3)	0.4302(2)	0.1220(2)
N(1)	0.1024(2)	0.0088(2)	0.4013(1)
N(21)	−0.2834(2)	−0.1692(2)	0.0888(1)
N(22)	−0.2876(2)	0.0780(2)	0.0151(1)
N(31)	0.3343(2)	0.2114(2)	0.1896(1)
N(32)	0.0425(2)	0.2803(2)	0.0730(1)
N(41)	−0.1602(2)	0.3762(2)	0.4015(1)
N(42)	−0.2088(2)	0.3678(2)	0.1850(2)
N	0.4362(2)	−0.3103(2)	0.3189(1)
C(111)	0.5672(3)	−0.2148(2)	0.3123(2)
C(112)	0.7268(3)	−0.2590(3)	0.3457(2)
C(121)	0.4214(3)	−0.4457(2)	0.2519(2)
C(122)	0.3805(3)	−0.4462(3)	0.1336(2)
C(131)	0.4691(3)	−0.3333(3)	0.4329(2)
C(132)	0.4828(3)	−0.2117(3)	0.5140(2)
C(141)	0.2860(3)	−0.2487(2)	0.2783(2)
C(142)	0.1390(3)	−0.3292(3)	0.2764(2)

4. X-ray Structure of $[NEt_4]_2[Fe_4(\mu_3\text{-}S)_3(NO)_7]$ and $[NEt_4][Fe_4(\mu_3\text{-}S)_3(NO)_7]$. The fractional atomic coordinates of the mono- and dianion are reported in Tables II and III, respectively. Selected interatomic distances within the mono- and dianion are compared in Table IV. An ORTEP drawing of the structure of the $[Fe_4(\mu_3\text{-}S)_3(NO)_7]^-$ monoanion with the adopted labeling scheme is shown in Figure 6. The overall geometry of the monoanion is also representative of that of the $[Fe_4(\mu_3\text{-}S)_3(NO)_7]^{2-}$ dianion. The structure of $[Fe_4(\mu_3\text{-}S)_3(NO)_7]^-$, in its monohydrated cesium salt, has been the object of a pioneering structural determination by Johansonn and Lipscomb[8] and subsequently reinvestigated as the tetraphenylarsonium salt by Chu and Dahl.[9] Owing to the much greater precision, only data of the latter have been used for comparison in the following discussion.

The architecture of $[Fe_4(\mu_3\text{-}S)_3(NO)_7]^-$ has been described as being composed of a trigonal pyramid of four Fe atoms with both triply-bridging S atoms and a Fe–Fe bonds linking an apical Fe(NO) fragment to three basal $Fe(NO)_2$ moieties, which are connected to one another by the three triply bridging sulfur atoms (but no Fe–Fe bonds).[9] The idealized symmetry is C_{3v}. An alternate description of the anion is based on an Fe_3S_3 hexaring with a chair conformation; each iron atom binds two nitrosyl groups, three of which are in equatorial and three in axial positions. This hexaring moiety is capped on one side by an almost linear Fe(NO) fragment linked to all the three Fe and S atoms.

A comparison of the geometrical parameters of the monoanion with those of the same anion in its tetraphenylarsonium salt reported by Chu and Dahl clearly shows that packing effects are rather relevant in determining significant distortions of the Fe_4S_3 core. For instance the Fe(1)–Fe(2,3,4) distances range from 2.695 (1) to 2.704 (1) Å with two short and one long distances in $[NEt_4][Fe_4(\mu_3\text{-}S)_3(NO)_7]$, whereas in $[AsPh_4][Fe_4(\mu_3\text{-}S)_3(NO)_7]$ the range is spread from 2.683 (2) to 2.708 (2) Å with one short and two long distances. The relevance of the cation in affecting the individual molecular parameters of the $[Rh_6(CO)_{15}C]^{2-}$ counteranion has been documented,[23] and packing effects have been recently ascertained in the related $Fe_4(\mu_3\text{-}S)_4(\eta^5\text{-}$

Table III. Fractional Atomic Coordinates of Non-hydrogen Atoms (Esd's in Parentheses) for $[NEt_4]_2[Fe_4S_3(NO)_7]$

atom	x	y	z
Fe(1)	0.4433(1)	0.06381(8)	0.77666(7)
Fe(2)	0.2238(1)	0.11366(9)	0.82805(7)
Fe(3)	0.2456(1)	0.04614(9)	0.64847(7)
Fe(4)	0.4421(1)	0.20822(9)	0.72350(7)
S(1)	0.2473(2)	0.0069(2)	0.7655(1)
S(2)	0.4267(2)	0.1700(2)	0.8382(1)
S(3)	0.4531(2)	0.0988(2)	0.6622(1)
O(1)	0.6579(6)	-0.0327(5)	0.8403(4)
O(21)	0.1862(7)	0.0901(5)	0.9736(4)
O(22)	-0.0037(7)	0.1920(5)	0.7502(5)
O(31)	0.207(1)	-0.0729(6)	0.5489(5)
O(32)	0.0346(7)	0.1435(5)	0.5836(4)
O(41)	0.6701(8)	0.2993(6)	0.7446(5)
O(42)	0.2214(9)	0.2942(5)	0.6509(4)
N(1)	0.5701(6)	0.0086(5)	0.8149(4)
N(21)	0.2146(7)	0.0935(5)	0.9147(4)
N(22)	0.0970(7)	0.1615(5)	0.7785(4)
N(31)	0.2383(9)	-0.0273(5)	0.5962(4)
N(32)	0.1247(7)	0.1082(5)	0.6171(4)
N(41)	0.5855(8)	0.2545(5)	0.7388(4)
N(42)	0.3088(8)	0.2546(5)	0.6820(4)
N(100)	-0.2240(6)	0.3425(5)	0.5281(4)
N(200)	0.2228(7)	0.0982(5)	0.3776(4)
C(111)	-0.3047(9)	0.3827(7)	0.5764(5)
C(112)	-0.4591(9)	0.3814(8)	0.5443(6)
C(121)	-0.239(1)	0.3886(7)	0.4550(5)
C(122)	-0.159(1)	0.3552(9)	0.4009(5)
C(131)	-0.0753(9)	0.3398(7)	0.5726(6)
C(132)	-0.0153(9)	0.4193(6)	0.5945(6)
C(141)	-0.272(1)	0.2615(6)	0.5079(6)
C(142)	-0.281(1)	0.2110(7)	0.5757(6)
C(211)	0.122(2)	0.1430(8)	0.3237(9)
C(212)	-0.013(2)	0.136(1)	0.342(1)
C(221)	0.237(2)	0.1251(9)	0.4561(6)
C(222)	0.269(1)	0.2100(7)	0.4708(6)
C(231)	0.343(1)	0.121(1)	0.349(1)
C(232)	0.466(2)	0.090(1)	0.391(2)
C(241)	0.191(1)	0.0146(7)	0.3739(7)
C(242)	0.168(1)	-0.0221(7)	0.2961(5)

$C_5H_5)_4$ on simple substitution of the cyclopentadienyl with the methylcyclopentadienyl moiety.[24] Nevertheless, even if the structure determination of $[Fe_4S_3(NO)_7]^-$ in its tetraphenylarsonium salt is less accurate than that of the corresponding NEt_4^+ salt, the average Fe–Fe and Fe–S distances are in excellent agreement with each other (in most cases within 1σ). Compare, for instance the average value of 2.698 vs 2.700 Å for the Fe(1)–Fe(2,3,4) interactions, 3.573 vs 3.570 Å for the Fe···Fe interactions, 2.210 vs 2.206 Å for the Fe(1)–S interactions, and 2.257 vs 2.258 Å for the remaining Fe–S interactions.

Passing from the monoanion to the dianion in their NEt_4^+ salts, the increase of the charge by addition of an extra electron is reflected in a variation of the geometrical parameters of both the Fe_4S_3 core and the nitrosyl interactions. For instance, the average Fe(1)–Fe(2,3,4) bond length increases from 2.698 to 2.764 Å, and a parallel, although less pronounced, increment is observed for the Fe(1)–S interactions (from 2.210 to 2.226 Å) and the remaining Fe–S bond lengths (from 2.257 to 2.272 Å). The above changes suggest that the single occupied molecular orbital (SOMO) of the dianion has an antibonding character both for the Fe–Fe and Fe–S interactions which is larger for the former. In addition, the departure from an idealized C_{3v} toward a C_s symmetry is enhanced as shown, for instance, by the difference in length of the longest Fe–Fe bonding interaction with respect to the other two (0.026 vs 0.009 Å) in the two salts. However, it is worth remarking that the spreading of the Fe–Fe bond distances in $[NEt_4]_2]Fe_4(\mu_3\text{-}S)_3(NO)_7]$ and $[AsPh_4][Fe_4(\mu_3\text{-}S)_3(NO)_7]$ are comparable and this suggests that in these compounds packing forces can be as relevant as the Jahn–Teller effect arising from population with one electron of a doubly degenerate energy level (see later).

Table IV. Selected Interatomic Distances (Å) and Angles (deg) with Esd's in Parentheses

	$[NEt_4][Fe_4S_3(NO)_7]$	$[NEt_4]_2[Fe_4S_3(NO)_7]$
Fe(1)–Fe(2)	2.695 (1)	2.781(1)
Fe(1)–Fe(3)	2.704(1)	2.757(1)
Fe(1)–Fe(4)	2.696(1)	2.753(1)
Fe–Fe_{av}	2.698	2.764
Fe(2)···Fe(3)	3.564(1)	3.584(1)
Fe(2)···Fe(4)	3.590(1)	3.683(1)
Fe(3)···Fe(4)	3.566(1)	3.609(1)
Fe···Fe_{av}	3.573	3.625
Fe(1)–S(1)	2.209(1)	2.216(2)
Fe(1)–S(2)	2.207(1)	2.233(2)
Fe(1)–S(3)	2.213(1)	2.230(2)
Fe(1)–S_{av}	2.210	2.226
Fe(2)–S(1)	2.251(1)	2.267(2)
Fe(2)–S(2)	2.254(1)	2.277(2)
Fe(3)–S(1)	2.248(1)	2.269(2)
Fe(3)–S(3)	2.265(1)	2.284(2)
Fe(4)–S(2)	2.254(1)	2.266(2)
Fe(4)–S(3)	2.262(1)	2.271(2)
Fe–S_{av}	2.257	2.272
S(1)···S(2)	3.554(1)	3.533(3)
S(1)···S(3)	3.554(1)	3.553(2)
S(2)···S(3)	3.562(1)	3.560(2)
S···S_{av}	3.557	3.549
Fe(1)–N(1)	1.661(2)	1.653(7)
Fe(2)–N(21)	1.669(2)	1.665(7)
Fe(2)–N(22)	1.673(2)	1.644(7)
Fe(3)–N(31)	1.667(2)	1.618(7)
Fe(3)–N(32)	1.669(2)	1.662(7)
Fe(4)–N(41)	1.668(2)	1.652(7)
Fe(4)–N(42)	1.665(2)	1.629(7)
Fe–N_{av}	1.667	1.646
N(1)–O(1)	1.163(2)	1.172(6)
N(21)–O(21)	1.159(3)	1.191(7)
N(22)–O(22)	1.156(2)	1.176(7)
N(31)–O(31)	1.166(2)	1.181(8)
N(32)–O(32)	1.159(2)	1.169(7)
N(41)–O(41)	1.165(2)	1.165(7)
N(42)–O(42)	1.158(3)	1.181(7)
N–O_{av}	1.161	1.176
S(1)–Fe(1)–S(2)	107.15(2)	105.12(7)
S(1)–Fe(1)–S(3)	106.96(2)	106.13(7)
S(2)–Fe(1)–S(3)	107.38(2)	105.80(8)
S(1)–Fe(2)–S(2)	104.17(2)	102.06(7)
S(1)–Fe(3)–S(3)	103.91(2)	102.61(7)
S(2)–Fe(4)–S(3)	104.13(2)	103.34(8)
Fe(2)–S(1)–Fe(3)	104.79(2)	104.43(9)
Fe(1)–S(1)–Fe(2)	74.33(2)	76.69(7)
Fe(1)–S(1)–Fe(3)	74.70(2)	75.86(6)
Fe(2)–S(2)–Fe(4)	105.57(2)	108.31(7)
Fe(1)–S(2)–Fe(2)	74.32(2)	76.13(7)
Fe(1)–S(2)–Fe(4)	74.35(2)	75.42(7)
Fe(3)–S(3)–Fe(4)	103.93(2)	104.79(8)
Fe(1)–S(3)–Fe(3)	74.28(2)	75.28(7)
Fe(1)–S(3)–Fe(4)	74.08(2)	75.40(7)
Fe(1)–N(1)–O(1)	178.3(2)	177.6(6)
Fe(2)–N(21)–O(21)	168.0(2)	165.8(6)
Fe(2)–N(22)–O(22)	167.3(2)	170.4(6)
Fe(3)–N(31)–O(31)	165.6(2)	164.8(8)
Fe(3)–N(32)–O(32)	166.9(2)	167.5(6)
Fe(4)–N(41)–O(41)	163.6(2)	166.3(8)
Fe(4)–N(42)–O(42)	167.2(2)	172.8(7)

The expected effect of a major back-donation in the dianion is only evident on comparing $[Fe_4S_3(NO)_7]^-$ and $[Fe_4S_3(NO)_7]^{2-}$ in their NEt_4^+ salts and is clearly manifest from the shortening of the Fe–N interaction in the dianion (1.646 vs 1.667 Å in the monoanion) and a corresponding lengthening of the average NO distance (1.176 vs 1.161 Å). The Fe–N–O angles in the dianion are spread in the 164.8(8)–177.6(6)° range (average angle 169.3°,

(23) Albano, V. G.; Braga, D.; Grepioni, F. *Acta Crystallogr.* **1989**, *B45*, 60.
(24) Blonk, H. L.; van der Linden, J. G. M.; Steggerda, J. J.; Geleyn, R. P.; Smits, J. M. M.; Beurskens, G.; Beurskens, P. T.; Jordanov, J. *Inorg. Chem.* **1992**, *31*, 957.

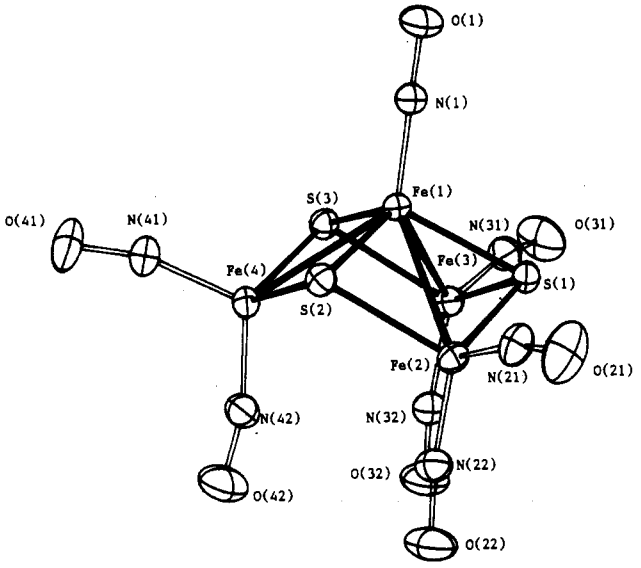

Figure 6. ORTEP drawing of the structure of the $[Fe_4S_3(NO)_7]^-$ monoanion, which is also representative of that of the corresponding $[Fe_4S_3(NO)_7]^{2-}$ dianion.

vs 168.1° in the monoanion), and no individual nitrosyl group can be considered as bent.[9]

5. Extended Huckel Molecular Orbital Calculations on $[Fe_4(\mu_3\text{-}S)_3(NO)_7]^n$ (n = 1, 2) and Possible Interpretation of the EPR Spectral Behavior of $[Fe_4(\mu_3\text{-}S)_3(NO)_7]^{2-}$. Extended Huckel molecular orbital (EHMO) calculations on $[Fe_4(\mu_3\text{-}S)_3(NO)_7]^-$ have already been performed by Hoffman.[25] Under C_{3v} idealized symmetry, the HOMO has A_1 symmetry and is substantially nonbonding with respect to the Fe–Fe interactions, whereas the LUMO is of E symmetry and is antibonding. Unfortunately the contribution of the nitrosyl ligands to the LUMO was not reported in details. With the aim to gather some more insight into the nature of the two suggested $[Fe_4(\mu_3\text{-}S)_3(NO)_7]^{2-}$ isomers and to interpret their EPR features, we have repeated EHMO calculations on $[Fe_4(\mu_3\text{-}S)_3(NO)_7]^-$ and $[Fe_4(\mu_3\text{-}S)_3(NO)_7]^{2-}$ by using CACAO.[26] The most significant results can be summarized as it follows: The $[Fe_4(\mu_3\text{-}S)_3(NO)_7]^-$ monoanion with an idealized C_{3v} symmetry shows a LUMO which is a doubly degenerate level also when the nitrosyl groups are included in the calculation. This e level is made by the 39th and 40th MO (the MO numbers are assigned starting from the highest unoccupied MO) and is antibonding (or nonbonding) in character for the miscellaneous Fe–Fe, Fe–S, Fe–N, and N–O interactions. Occupation of this level with an electron, as it occurs in $[Fe_4(\mu_3\text{-}S)_3(NO)_7]^{2-}$, should result into a lengthening of the Fe–Fe interactions and a loss of degeneracy through a distortion along one of the E vibrational mode giving rise to an ion of C_s idealized symmetry. A comparison of the solid-state structure of $[Fe_4(\mu_3\text{-}S)_3(NO)_7]^{2-}$ and $[Fe_4(\mu_3\text{-}S)_3(NO)_7]^-$, in their $[NEt_4]^+$ salts, confirms this conclusion since it shows a lengthening of the three Fe–Fe interactions and a significant reduction of the idealized symmetry from C_{3v} to C_s (see Table IV).

Simulation of a $C_{3v} \rightarrow C_s$ distortion according to what is experimentally found in the $[Fe_4(\mu_3\text{-}S)_3(NO)_7]^-$ and $[Fe_4(\mu_3\text{-}S)_3(NO)_7]^{2-}$ molecular ions splits the LUMO level in lower (40th MO, 39a′) and higher energy (39th MO, 27a″) orbitals. The 40th MO (39a′) receives significant contributions only from two axial nitrosyls (Figure 7a). As a result, a $[Fe_4(\mu_3\text{-}S)_3(NO)_7]^{2-}$ molecular ion having this stereogeometry should show an EPR signal consisting of a 1:2:3:2:1 quintet by coupling of the unpaired electron with two equivalent nitrogen atoms. This is the case of the species formerly labeled as B, which is the one prevailing in THF or also in acetonitrile in the presence of a high concentration of Na^+ ions.

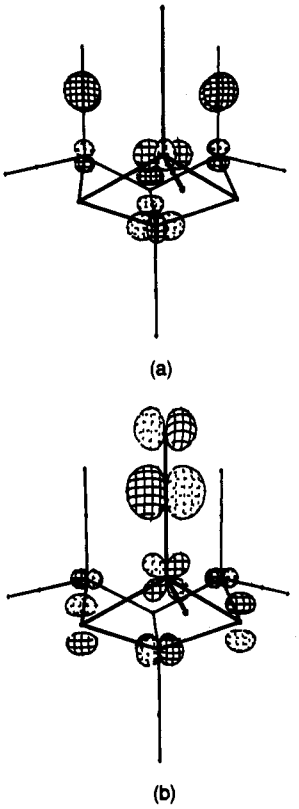

Figure 7. CACAO[26] plots of the orbitals 39a′ (a) and 27a″ (b). Fe–Fe bonds, as well as atomic orbital contributing less than 3% to the above MO's, have been omitted for clarity.

On the contrary, simulation of the above $C_{3v} \rightarrow C_s$ conversion through other kind of distortions such as, for instance, elongation of two Fe–Fe interactions, causes the stabilization of the 39th (27a″) molecular orbital. This, as stated above, receives contribution mainly from only one axial nitrosyl group (Figure 7b). Occupation of this orbital with one electron should correspond with the observation of a 1:1:1 triplet in the EPR spectrum, as it occurs for the species formerly labeled as A. The measured coupling constants of the triplet and quintet (5.0 ± 0.5 and 2.7 ± 0.5 G, respectively) qualitatively follow the trend suggested by the EHMO calculations which indicate a greater contribution (16%) to the 27a″ SOMO of the p orbitals of the nitrogen atom of an axial nitrosyl group and an inferior contribution (11%) to the 39a′ SOMO of the p orbitals of the remaining two axial nitrogen atoms. In view of this and the experimental observations reported in the previous sections, it appears possible to conclude that both species A and B could be intact $[Fe_4(\mu_3\text{-}S)_3(NO)_7]^{2-}$ molecular ions slightly differing in their stereogeometry.

Experimental Section

All reactions including sample manipulations were carried out with standard Schlenk techniques under nitrogen in dried solvents. The $[Fe_4S_3(NO)_7]^-$ salts were prepared according to literature methods,[16,17] and analyses have been performed as follows. The iron content has been measured by atomic absorption, and NEt_4^+ has been gravimetrically determined as the BPh_4^- salt. Infrared spectra were recorded on a Perkin-Elmer 1605 interferometer using CaF_2 cells. Proton NMR spectra were recorded on a Bruker WP-200 spectrometer, and EPR spectral measurements have been carried out on a Varian E-104 spectrometer. Typically, EPR experiments were carried out on using molar concentrations in the range 10^{-3}–10^{-5} M, with microwave power set at 5 mW and modulation amplitudes of 1.5/5 and 0.5–0.05/1 Gpp, respectively, for glass and fluid samples. Materials and apparatus for the electrochemical measurements have been described elsewhere.[27] Potential values

(25) Sung, S. S.; Glidewell, C.; Butler, A. R.; Hoffmann, R. *Inorg. Chem.* **1985**, *24*, 3856.
(26) Proserpio, D. M.; Mealli, C. *J. Chem. Ed.* **1990**, *67*, 399.

Table V. Crystallographic Data for $[NEt_4][Fe_4S_3(NO)_7]$ and $[NEt_4]_2[Fe_4S_3(NO)_7]$

chem formula	$C_8H_{20}Fe_4N_8O_7S_3$	$C_{16}H_{40}Fe_4N_9O_7S_3$
fw	659.88	790.13
space group	$P\bar{1}$	$P2_1/c$
a (Å)	9.161(4)	10.248(3)
b (Å)	10.254(2)	17.814(8)
c (Å)	13.480(4)	18.475(4)
α (deg)	97.71(2)	90
β (deg)	109.86(3)	103.33(3)
γ (deg)	94.82(2)	90
V (Å^3)	1169(1)	3282(3)
Z	2	4
ρ_{calc} (g·cm^{-3})	1.875	1.599
μ (cm^{-1})	27.37	19.64
transm coeff	0.80	0.87
final R and R_w indices[a]	0.018, 0.026	0.045, 0.058

[a] $R = [\sum(|F_o| - k|F_c|)/\sum|F_o|]$, $R_w = [\sum w(|F_o| - k|F_c|)^2/\sum w|F_o|^2]^{1/2}$.

are referred to the saturated calomel electrode (SCE). Under the present experimental conditions the ferrocenium–ferrocene couple was located at +0.38 V in acetonitrile, +0.45 V in CH_2Cl_2, and +0.54 V in THF solution. At 0.2 V·s^{-1}, the relevant peak-to-peak separations were 73, 80, and 138 mV, respectively.

1. Synthesis of $[NEt_4][Fe_4S_3(NO)_7]$. A crystalline sample of $K[Fe_4S_3(NO)_7]\cdot 2H_2O$ (7.45 g), obtained according to literature methods,[18] was dissolved in methanol (50 mL) and treated under stirring with a solution of 4 g of $[NEt_4]Br$ in methanol (20 mL). The resulting microcrystalline precipitate was filtered out, dried in vacuum, and extracted in THF (50 mL). Precipitation by slow diffusion of toluene (80 mL) gave well-shaped crystals of $[NEt_4][Fe_4S_3(NO)_7]$ in ca. 70% yields. [Anal. Found: NEt_4^+, 19.2; Fe, 33.4. Calc for $[NEt_4][Fe_4S_3(NO)_7]$: NEt_4^+, 19.71; Fe, 33.88.]

2. Synthesis of $[NEt_4]_2[Fe_4S_3(NO)_7]$. A crystalline sample of $[NEt_4][Fe_4S_3(NO)_7]$ (1.51 g) was dissolved in anhydrous THF (20 mL) and reduced by addition in portions of a THF solution of sodium diphenyl ketyl (0.5 M) while being monitored by IR. The resulting brown suspension was filtered, and the microcrystalline precipitate was washed with THF, dried under vacuum, and extracted in the minimum amount of anhydrous acetonitrile (ca. 10 mL). The dark brown solution was precipitated by slow diffusion of diisopropyl ether (30 mL) to give 0.87 g of well-shaped black crystals of $[NEt_4]_2[Fe_4S_3(NO)_7]$. These are soluble in acetone and acetonitrile and sparingly soluble or insoluble in THF and nonpolar solvents. [Anal. Found: NEt_4^+, 33.8; Fe, 28.3. Calc for $[NEt_4]_2[Fe_4S_3(NO)_7]$: NEt_4^+, 34.24; Fe, 29.42.]

3. Attempted Preparation of $[NEt_4]_3[Fe_4S_3(NO)_7]$. $[NEt_4][Fe_4S_3(NO)_7]$ (0.82 g) was dissolved in THF (20 mL) and treated with ca. 2.5 equiv of sodium naphthalenide while being monitored by infrared. The resulting brown suspension was filtered, and the precipitate was dissolved in dried acetonitrile to obtain a brown solution containing a mixture of $[Fe_4S_3(NO)_7]^{3-}$ and $[Fe_4S_3(NO)_7]^{2-}$ (ca. 10% relative abundance from infrared nitrosyl absorptions). Precipitation of this solution by slow diffusion of diisopropyl ether afforded a waxy precipitate mainly consisting of $[NEt_4]_2[Fe_4S_3(NO)_7]$ on the basis of its infrared absorptions.

4. X-ray Data Collection and Structure Determination of $[NEt_4][Fe_4S_3(NO)_7]$ and $[NEt_4]_2[Fe_4S_3(NO)_7]$. Crystal data and other experimental details are summarized in Table V. Two black crystals of $[NEt_4][Fe_4S_3(NO)_7]$ (0.12 × 0.15 × 0.20 mm) and $[NEt_4]_2[Fe_4S_3(NO)_7]$ (0.15 × 0.15 × 0.25 mm) were coated with cyanoacrylate glue for protection from aerial oxidation and mounted on a glass fiber. The diffraction experiments were carried out on an Enraf-Nonius CAD-4 diffractometer at room temperature, using graphite-monochromatized Mo Kα radiation (λ = 0.710 73 Å). The diffracted intensities were corrected for Lorentz, polarization, and absorption (empirical correction)[28] but not for extinction. A decay correction was also applied to the data of the dianion (maximum decay ca. 30% on F_o). Scattering factors for all the atomic species and anomalous dispersions corrections for scattering factors of non-hydrogen atoms were taken from ref 29. Both structures were solved by direct methods (MULTAN) and refined by full-matrix least squares, minimizing the function $\sum w(|F_o| - k|F_c|)^2$.

An anisotropic thermal parameter was assigned to all the non-hydrogen atoms. For $[NEt_4][Fe_4S_3(NO)_7]$ the hydrogen atoms of the cation were introduced in the structure model at calculated positions (C–H = 0.95 Å) but not refined. In $[NEt_4]_2[Fe_4S_3(NO)_7]$, owing to the high value of the thermal parameter of the carbon atoms of the cations (deriving from a situation of partial disorder), the contribution of the H atoms was not taken into account. The final difference Fourier synthesis showed maxima residuals of 0.57 and 0.89 e/Å^3 for the monoanion and the dianion, respectively. The final atomic coordinates are listed in Tables II and III. All the calculations were performed on a PDP11/73 computer using the SDP-Plus Structure Determination Package 3.[30]

Acknowledgment. We wish to acknowledge the EEC (Contract ST2J-0479) and the MURST for financial assistance and thank Dr. C. Mealli for making available the CACAO program.

Supplementary Material Available: Tables of crystal structure analyses, atomic coordinates of all atoms, and anisotropic and isotropic thermal parameters of all non-hydrogen atoms for $[NEt_4][Fe_4S_3(NO)_7]$ and $[NEt_4]_2[Fe_4S_3(NO)_7]$ and MO diagrams for C_{3v} $[Fe_4S_3(NO)_7]^-$ (Figures S1 and S2) and C_s $[Fe_4S_3(NO)_7]^{2-}$ (Figure S3) (8 pages). Ordering information is given on any current masthead page.

(27) Osella, D.; Ravera, M.; Nervi, C.; Housecroft, C. E.; Raithby, P.; Zanello, P.; Laschi, F. *Organometallics* **1991**, *10*, 3253.

(28) North, A. C.; Phillips, D. C.; Mathews, F. S. *Acta Crystallogr.* **1968**, *A24*, 351.

(29) *International Tables for X-ray Crystallography*; The Kynoch Press: Birmingham, U.K., 1974; Vol. IV.

(30) B. A. Frenz, and Associates. SDP Plus Version 1.0, Enraf-Nonius, Delft, The Netherlands, 1980.